PROGRESS IN PHOTOVOLTAICS: RESEARCH AND APPLICATIONS
Prog. Photovolt: Res. Appl. (2015)
Published online in Wiley Online Library (wileyonlinelibrary.com). DOI: 10.1002/pip.2595

RESEARCH ARTICLE

Impact of light soaking and thermal annealing on amorphous silicon thin film performance

M. Pierro, F. Bucci and C. Cornaro*

Department of Enterprise Engineering, CHOSE, University of Rome "Tor Vergata", Via del Politecnico, 1, 00133 Rome, Italy

ABSTRACT

Nowadays, there is a wide debate in literature related to the silicon thin films seasonal performance. Amorphous modules seem to react positively to the temperature, while the temperature parameters indicate a negative thermal response. Periodic fluctuations of nominal power due to light soaking and thermal annealing effects are observed. On the other hand, the module temperature reached in some open rack plants seems too low to activate annealing power regeneration process so that the seasonal performance trend may depend mainly on other effects such as spectral or irradiance. In the following paper, a model that allows to calculate the impact of all the phenomena that affect the photovoltaic performance is used. The light soaking and thermal annealing contributions are measured from outdoor data using two different methods. Both methods lead to similar results, and the model is able to reproduce the seasonal performance with an acceptable level of reliability on the day, hour, minute time scale. An analysis of each effect contribution to the seasonal performance is also provided. Thus, main open questions related to a-Si thin films performance such as positive reaction to temperature and seasonal fluctuations are discussed. Copyright © 2015 John Wiley & Sons, Ltd.

KEYWORDS
light soaking; thermal annealing; amorphous silicon; outdoor monitoring

***Correspondence**
C. Cornaro, Department of Enterprise Engineering, CHOSE, University of Rome "Tor Vergata", Via del Politecnico, 1, 00133 Rome, Italy.
E-mail: cornaro@uniroma2.it

Received 28 March 2013; Revised 8 July 2014; Accepted 30 December 2014

1. INTRODUCTION

Nowadays, there is a wide debate in literature related to the silicon thin films seasonal performance. Amorphous modules seem to react positively to the temperature, while the temperature parameters indicate a negative thermal response. Using statistical methods [1] the power thermal coefficients of amorphous and crystalline modules have been measured on hourly and daily time scale. The crystalline one does not change while the amorphous coefficients are negative if measured on a hourly basis and positive if measured on a daily basis.

Periodic fluctuations of nominal power due to light soaking (LS) and thermal annealing (TA) effects are observed. These degradations and regenerations of the nominal power contribute to the Performance Ratio (PR) seasonal behavior [2,3]. How much these effects are important with respect to the others is still not clear. Recently, [4] and [5] tried to estimate these effects contribution.

Moreover, the module temperature reached in some open rack plants seems too low to activate annealing power regeneration process. Thus, the PR seasonal behavior is difficult to explain. King *et al.* [2] propose two possible degradation phases: an initial degradation that requires high annealing temperature to be recovered (Tcell $> 80°C$), as also found in laboratory experiments [4], and a second weak degradation phase that appears near the power stabilization level that could be easily reversed by an annealing process at low activation temperature (Tcell $> 40°C$). J. M. Pearce *et al.* [6], investigate on two different light-induced defect states: "fast" and "slow" states. The defect states that are created faster can be annealed faster also at room temperature. Lately, M. Nikolaeva-Dimitrova *et al.* in [7] measured the velocity of the LS and TA process, thus, the threshold temperature for the TA effect could result from the LS intensity and TA exponential rate. In [5], a small power regeneration has been measured at $25°C$ degree in dark condition. On the other hand the seasonal performance ratio trend may depend mainly on other effects such as irradiance [8] and spectral effect [3,9–11].

In the following paper, the model presented in [12] is improved by refining the method to measure the LS and

TA contribution to the performance of a double junction amorphous silicon module. The impact of these effects is evaluated using outdoor data implementing two different methods. The first allows to evaluate the direct impact of these phenomena on the temperature response trying to explain the inversion of the amorphous thin films thermal behavior at the seasonal level. The second method provides a direct evaluation of the LS and TA contributions. Both methods lead to similar results, and the model is able to reproduce the seasonal performance on a daily, hourly, and minute time scale. An analysis of each effects contribution to the seasonal performance is also provided. It appears that in the reporting real operating conditions (ROC), LS and TA effects play important roles in the performance behavior because, together with spectral and temperature effects, they produce both the minimum and maximum seasonal performance. It was confirmed in a quantitative way that the increase of the a-Si module performance in summer and the decrease in winter depend on the LS, TA and spectral effects that are able to compensate the negative intrinsic thermal response of the module. In Rome climatic conditions, low latitude and prevalent warm weather, the LS and TA are the dominant effects. On the contrary, in other sites with higher latitude or prevalent cold weather, the spectral effect could be the dominant one [3].

2. METHODOLOGY

When a photovoltaic module operates outdoor, its efficiency (η_{ROC}) is different from the nominal one that is measured in a laboratory at Standard Test Condition (η_{STC}). The main used parameter to evaluate the module performance in ROC is the performance ratio: $PR = \eta_{ROC}/\eta_{STC}$.

The phenomena that produce a PR variation are the following: spectral, reflection, temperature and irradiance effects. These effects take into account the change of the module performance when the climatic conditions differ from the STC ones: irradiance spectrum $AM_0 = 1.5G$, angle of incidence $\theta_0 = 0$, cell temperature $T_0 = 25°C$ and irradiance $G_0 = 1000\ W/m^2$. In addition, the PR could be modified also by the nominal power variation, resulting in a different η_{STC} from the one declared by the module manufacturer. This phenomenon includes possible errors in nominal power measurement, initial or long term power degradation or seasonal power fluctuation due to LS and TA effects.

In [12], each effect was separately modeled through a parametric function of the climatic conditions: air mass, angle of incidence (*AOI*), cell temperature and plane of array irradiance. Such functions represent the module performance ratio with respect to each specific phenomena. Thus, the modeled overall performance ratio results from the product of these five performance factors: the spectral, reflection, temperature and irradiance performance and nominal power variation. Comparing the daily performance measured and calculated by this semi-empirical model, a very good agreement is reached for the crystalline module, while a worse result for the amorphous thin film was realized. In this work, the model is improved by refining the methods to evaluate the LS and TA using outdoor data.

In this section, the experimental setup and the data set used to measure and validate the model are reported. The LS and TA effects are discussed and two different methods to measure the impact of these effects on the seasonal performance are described. Then the PR measurement procedures and the PR modellization are summarized. Finally, the PR and losses analysis technique used to study the seasonal behavior are described.

2.1. Experimental setup and data sets

The Device Under Test (DUT) is an amorphous thin film (a-Si): EPV50 (Energy Photovoltaics, Inc., Robbinsville, NJ, USA) with a nominal power (P_n)declared by the manufacturer of $50W_p$.The module is a double junction device (a-Si:H/a-Si:H) bottom limited with $J_{top} = 6,65\ mA/cm^2$ and $J_{bottom} = 6,01\ mA/cm^2$.The Quantum Efficiency (QE) of EPVsolar cell 2760-1 measured at the National Renewable Energy Laboratory is reported in [12].

The measurements were taken at the Ester Laboratory, University of Rome "Tor Vergata", Italy [13]. The DUT was connected to an maximum power point tracker (MPPT), and I, V, P (at mmp) were collected every minute while the IV curves were traced every ten minutes. Simultaneously, the main climatic variables were collected every minute: global (plane of array and horizontal) and diffuse irradiance by pyranometers, direct normal irradiance by a pyrheliometer, air and back of the module temperature by a PT100 and wind speed and direction by an anemometer.

In this work, two data sets were used:

- 18 months data (from 1 May 2009 to 10 October 2010) from ROC monitoring of the module with south orientation and monthly optimal tilt (each month the DUT tilt was changed to maximize the delivered energy)
- 2 months data (from 10 June 2011 to 27 July 2011) coming from the ROC monitoring of the module on a tracker station.

2.2. Light soaking and thermal annealing measurement methods

In the hydrogenated amorphous silicon thin film (a-Si:H), the LS produces an increasing of the a-Si dangling bonds in the intrinsic layer resulting in a module power degradation. This degradation acts on a monthly time scale and reaches a maximum (stabilized power), which depends on the number of junctions (initial degradation). On the other hand, the TA process promotes the a-Si:H bonds recombination, reducing the trap states inside the p/i/n

junction. This produces a partial regeneration of the light-degraded power. LS seems to depend on the cumulative energy absorbed by the module while TA seems to produce a continuous power regeneration until the cell temperature remains above a threshold temperature. Even if the Staebler–Wronsky effect (SWE) usually refers only to the light-induced metastable changes in the photoconductivity of the a-Si:H [14], for brevity in this paper, the combined action of LS and TA is called Staebler–Wronsky effect. This effect essentially modifies the nominal fill factor on the daily time scale and affects the module power in a cumulative way that depends on the module history of absorbed irradiance and reached cell temperature. Thus, for amorphous silicon thin film, the nominal power could not be considered constant any more but daily dependent ($P_{m0}(day)$). The instantaneous performance ratio that includes spectral, angle of incidence (AOI), temperature and irradiance effects can be expressed as follows:

$$PR(t) = \frac{P_m(t)}{P_{m0}(day)} \frac{G_0}{G_i(t)} \tag{1}$$

where

- $P_m(t)$ is the module power at time t in the specific day;
- $P_{m0}(day)$ is the nominal power of the module measured in the specific day;
- $G_i(t)$ is the plane of array (POA) irradiance at time t in the specific day, and $G_0 = 1000\ \frac{W}{m^2}$ is the reference irradiance.

Because $P_{m0}(day)$ is the reference point for the performance ratio evaluation (Equation 1), this nominal power daily variation contributes to the PR seasonal behavior.

Moreover, because the a-Si nominal power depends on the temperature reached by the cells, its variation causes a changing of the seasonal thermal response of the module.

It is possible to model the SWE by two terms, one constant and one daily dependent:

1. ΔP_n takes into account the nominal power variation between the one declared by the manufacturer and the stabilized power deduced from outdoor data. It includes possible mismatch in nominal power laboratory measurements and differences between nominal and average STC power measured over the monitoring period. This factor produces a constant loss that it is called "Average degradation";
2. $PR_{SW}(day)$ (SW Performance Ratio) takes into account nominal power daily variation with respect to the average STC power measured over the monitoring period. It includes fluctuations of nominal power due to light-soaking degradation and thermal-annealing regeneration processes.

So that

$$\begin{aligned} P_{m0}(day) &= P_n \left(\frac{\langle P_{m0}\rangle}{P_n}\right)\left(\frac{P_{m0}(day)}{\langle P_{m0}\rangle}\right) = \\ &= P_n \Delta P_n PR_{SW}(day) \end{aligned} \tag{2}$$

- $\langle P_{m0}\rangle$ is the average nominal power deduced from outdoor data ($P_{m0}(day)$ averaged over all the monitoring period);
- P_n is the nominal power declared by the module manufacturer.

It is possible to evaluate the impact of SWE on the module seasonal performance using two different strategies. The first strategy is to split the SWE into two different contributions: one that takes into account the direct dependence of the nominal power on the cell temperature and the other that takes into account only the cumulative part of the nominal power variation. This approach is called the separate method (*SM*). The second strategy is to try to measure directly the relative nominal power variation. This approach is called the direct method (*DM*). A comparison between these two methods is reported in Section 3.

2.3. Performance ratio measurements and semi-empirical model

The overall performance is calculated as the product of five performance factors, each taking into account a different effect:

$$\begin{aligned} &PR(G_i, AM, \theta, T_{cell}, day) \\ &= \left(PR_{tn} PR_{am} PR_{aoi} PR_g\right)\left(\Delta P_n PR_{SW}\right) \end{aligned} \tag{3}$$

1. The PR_{tn} factor describes the performance of the module when the cell temperature is different from STC, and it is defined as the P_m variations with respect to the nominal Pn (measured at STC) when the spectrum, angle of incident and irradiance are fixed at $AM = AM_0$, $\theta = \theta_0$ and $G_i = G_0$. The temperature performance was modeled with a linear function of the cell temperature:

$$PR_{tn} = 1 + \gamma_n (T_{cell} - 25) \tag{4}$$

   The coefficient γ_n was provided by the module manufacturer, and $T_{cell} = T_{bom} + \Delta T_0 (G_i/G_0)$ where $\Delta T_0 = 3.6^{\circ}C$ is the difference between the back of the module temperature (T_{bom}) and the reference cell temperature measured at G_0.
2. The PR_{am} factor describes the performance of the DUT when the irradiance spectrum is different from STC, and it has been defined in [15] as the $\frac{Isc}{Gi}$ variation with respect to the nominal $\frac{Isc0}{G_0}$ (measured at STC) when the cell temperature and the AOI are fixed at $T_{cell} = T_0$ and $\theta = \theta_0$.

The spectral performance was modeled with a parametric function of POA direct and diffuse irradiance $\left(G_i^d \text{ and } G_i^{sh} = G_i - G_i^d\right)$, air mass ($AM$) and POA cloud ratio $\left(CRi = G_i^{sh}/G_i\right)$:

$$PR_{am} = \frac{Isc(G_i, AM, \theta_0, T_0)}{Gi} \Big/ \frac{Isc0}{G_0} \simeq \frac{AMM\,(AM)\,G_i^d + CRM\,(CR_i)\,G_i^{sh}}{G_i} \tag{5}$$

The function $CRM\,(CR_i)$ was called "Cloud Ratio Modifier", and it takes into account the spectral performance variation at different CR_i but at $AM = AM_0$, thus, it represents the response of the module performance to different diffuse irradiance spectra. It was evaluated using the $Isc(G_i, AM, \theta_0, T_{cell})$ tracker data after a temperature correction $\left(PR_t^{Isc}\right)$, and it was modeled by fitting the measurements with a linear function:

$$CRM(CR_i) = \frac{\left(\frac{Isc(G_i,AM,\theta_0,T_{cell})}{PR_t^{Isc}Gi} \Big/ \frac{Isc0}{G_0}\right) G_i - G_i^d}{G_i^{sh}} \simeq CA_0 + CA_1\,(CR_i) \tag{6}$$

The function $AMM\,(AM)$ was called "Air Mass Modifier", and it takes into account the spectral performance variation at different AM in very clear sky conditions (CRi less than 10%), thus, it represents the response of the module performance to different direct irradiance spectra. It was evaluated using the $Isc(G_i, AM, \theta_0, T_{cell})$ tracker data after a temperature correction $\left(PR_t^{Isc}\right)$, and it was modeled by fitting the measures with a polynomial function [15] :

$$AMM(AM) = \frac{\left(\frac{Isc(G_i,AM,\theta_0,T_{cell})}{PR_t^{Isc}Gi} \Big/ \frac{Isc0}{G_0}\right) G_i - CRM(CR_i) G_i^{sh}}{G_i^d} \simeq \sum_{n=0}^{4} CB_n\,(AM)^n \tag{7}$$

3. The PR_{aoi} factor describes the reflection performance of the DUT when the AOI is different from the STC, and it has been defined in [15] as the Isc variations with respect to the nominal $Isc0$ when the spectrum, cell temperature and irradiance are fixed at $AM = AM_0$, $T_{cell} = T_0$ and $G_i = G_0$.

   The reflection performance was modeled with a parametric function of POA direct irradiance $\left(G_i^d\right)$, POA diffuse irradiance $\left(G_i^{sh}\right)$ and the angle of incidence (θ):

$$PR_{aoi} = \frac{Isc(G_0, AM_0, \theta, T_0)}{Isc0} \simeq \frac{IAM\,(\theta)\,G_i^d + G_i^{sh}}{G_i} \tag{8}$$

   The function $IAM\,(\theta)$ was called "Incident Angle Modifier", and it takes into account the reflection performance variation at different θ, thus, it represents the response of the module performance to different AOI. It was evaluated using the $Isc(G_i, AM, \theta, T_{cell})$ fixed stand data, after providing spectrum, temperature and irradiance corrections $\left(PR_{am}, PR_t^{Isc}, G_i/G_0\right)$, and it was modeled by fitting the measurements by a polynomial function [15] :

$$IAM\,(\theta) = \frac{\left(\frac{Isc(G_i,AM,\theta,T_{cell})}{Isc_0\left(PR_{am}PR_t^{Isc}(G_i/G_0)\right)}\right) G_i - G_i^{sh}}{G_i^d} \simeq \sum_{n=0}^{5} CC_n\,(\theta)^n \tag{9}$$

4. The PR_g factor describes the performance of the module when the irradiance is different from STC, and it is defined as the $\frac{Pm}{Gi}$ variations with respect to the nominal $\frac{P_{m0}}{G_0}$ (measured at STC) when the spectrum, angle of incident and cell temperature are fixed at $AM = AM_0$, $\theta = \theta_0$ and $T_{cell} = T_0$.

   The irradiance performance was modeled with a nonlinear function of G_i/G_0:

$$\mathrm{PR}_g = \frac{P_m\,(G_i, AM_0, \theta_0, T_0)}{G_i} \Big/ \frac{P_{m0}}{G_0} \simeq \left[1 + C_1 \ln\left(\frac{G_i}{G_0}\right) + C_2 \left(\ln\left(\frac{G_i}{G_0}\right)\right)^2\right] \mathbf{C}_3 \tag{10}$$

   The coefficients $C_1$and C_2 were obtained fitting the measured data: $\left[\frac{V_m(G_i,AM,\theta,T_{cell})}{V_{m0}\left(PR_t^V\right)}\right]$ coming from the fixed stand versus $\ln\left(\frac{G_i}{G_0}\right)$. The coefficient C_3 was obtained fitting the measured data: $\left[\frac{I_m(G_i,AM,\theta,T_{cell})}{I_{m0}\left(\frac{G_i}{G_0}\right)\left(PR_t^I PR_{am} PR_{aoi}\right)}\right]$ coming from the fixed stand versus $\left(\frac{G_i}{G_0}\right)$. $PR_t^V$and PR_t^I factors are the temperature corrections of maximum power point voltage and current, and PR_{am}, PR_{aoi} factors are the spectral and reflection correction calculated from Equations 5 and 8.

5. The $(\Delta P_n PR_{SW})$ factor describes the nominal power variation that includes the average degradation and the SWE. The methods used to measure such a factor are reported in the next section.

2.4. Performance ratio and seasonal losses analysis

Once all the model parameters were estimated and the nominal power variation effect was measured, the overall daily PR measured and calculated was compared to validate both the model and the SWE measurement methods:

$$PR_m\,(day) = \frac{\sum_t Pm\,(t)}{Pn} / \frac{\sum_t G_i\,(t)}{G_0} \text{measured daily PR}$$
$$PR_c\,(day) = \frac{\sum_t PR\,(t)\,G_i\,(t)}{\sum_t G_i\,(t)} = \frac{\sum_t \left[\Pi_{i=1,5} PR_i\right] G_i\,(t)}{\sum_t G_i\,(t)} \text{calculated daily PR} \quad (11)$$

where t is the sampling rate (one minute), P_n is the module nominal power declared by the manufacturer, PR_i are the five aforementioned performance factors: $PR_{tn}, PR_{am}, PR_{aoi}, PR_g, (\Delta P_n PR_{SW})$.

In the same way, the overall daily losses and the losses related to each effect were calculated:

$$L\,(day) = 1 - \left[\frac{\sum_t PR\,(t)\,G_i\,(t)}{\sum_t G_i\,(t)}\right]$$
$$L_i\,(day) = 1 - \left[\frac{\sum_t PR_i\,(t)\,G_i\,(t)}{\sum_t G_i\,(t)}\right]$$

If $L_i\,(day)$ is positive, the effect produces a loss, otherwise, it produces a gain. Each $L_i\,(day)$ does not have a real physical meaning because, in real operating condition, all the effects occur simultaneously. Nevertheless, the loss fractions (**LFi**) were defined. The *LFi* fractions represent the impact of each effect on the overall daily losses:

$$LFi\,(day) = \frac{\left|L\,(day)\right|}{\left|\left(\sum_{i=1,5} L_i\right)\right|} L_i$$

Once calculated, the nominal power variation loss $L_{pv} = (1 - \Delta P_n PR_{SW})$ and the corresponding LF_{pv}, it is possible to define:

$$LF_{\Delta P_n} = (1 - \Delta P_n)$$
$$LF_{SW} = \left(LF_{pv} - LF_{\Delta P_n}\right)$$

where $LF_{\Delta P_n}$ is the loss fraction related to the average degradation, and LF_{SW} is the loss fraction related to the SWE. Considering that:

$$\left|L\,(day)\right| = \left|LF_{\Delta P_n} + LF_{SW} + LF_{am} + LF_{aoi} + LF_t + LF_g\right| \quad (12)$$

the seasonal impact of each effect on the overall losses can be quantified and analyzed through the daily behavior of the loss fractions.

The same analysis was carried out not only for each day but also for the whole monitoring period.

3. Staebler–Wronsky effect evaluation and discussion

In this section, the two methods of the SWE evaluation are described in details, and the obtained results are discussed. Then a comparison between the methods is reported. The SWE performance factor ($\Delta P_n PR_{SW}$) obtained by each method is used in the performance model described in Section 2. The calculated daily performance ratio shows a good agreement with the measured data. It appears that the direct method brings a better result with a greater correlation between measured and calculated daily PR. On the other hand, the separate method allows to measure and model the direct impact of the SWE on the seasonal thermal behavior of the module. It contributes to explain in a quantitative way, the apparent inversion of the module thermal response on the seasonal time scale [1].

Moreover, it should be remarked, that the reported performance model could be used for the performance analysis, but it cannot be used for the performance estimation of amorphous modules, because a parametric SWE model is not available at this stage. The separate model could be a first step in this direction.

3.1. Separate method

The SWE could be decomposed in two different contributions:

1. Temperature seasonal effect (*TSE*) modifies the module thermal response on a daily time scale and depends on maximum reached cell temperature. The TSE is in phase with the module temperature and could be described by a performance factor: $PR_{ts}\,(T_{\max}\,(day))$.
2. Power seasonal effect (*PSE*) modifies the module nominal power on a daily time scale and does not depend any more on module temperature and describes only the cumulative part of the SWE. Thus, the PSE is not in phase with temperature and could be described by a performance ratio: $PR_s\,(day)$.

Thus, the SW performance ratio could be expressed as:

$$PR_{SW} = PR_s PR_{ts}$$

Such decomposition could help to understand the SWE impact on the PR seasonal behavior. In this way, it is possible to explain why for the amorphous thin film, a positive influence of temperature on a seasonal time scale is observed, while negative junction power coefficients are measured. The impact of SWE on the seasonal thermal response of the module could be quantified. Thus, the effect of temperature on the seasonal performance behavior could be calculated and compared with the one observed for other module technologies not affected by the SWE. On the other hand, the power seasonal effect underlines the cumulative and competitive features of LS and TA effects.

This approach essentially improves the SWE evaluation method reported in [12], that in the present work is called "Average Method".

3.1.1. Temperature seasonal effect.

In the average method, the temperature effect on a seasonal time scale was directly evaluated through the thermal coefficient (γ_s) measured using the equation:

$$\begin{aligned} P_m(G_i, AM_0, \theta_0, T_{cell}) \frac{G_0}{G_i} &= \langle P_{m0} \rangle (1 + \gamma_s \Delta T_{cell}) \\ PR_t &= (1 + \gamma_s \Delta T_{cell}) \end{aligned} \tag{13}$$

where $P_m(G_i, AM_0, \theta_0, T_{cell})$ is the power at a fixed T_{cell} and $G_i \in \left\{950\frac{W}{m^2}; 1050\frac{W}{m^2}\right\}$, $\theta_0 \in \{0°; 5°\}$, $AM_0 \in \{1.2; 1.8\}$.

As reported in [12], for a crystalline module, the measured seasonal thermal coefficient (γ_s) is equal to the nominal thermal coefficient reported on the data sheet (γ_n). On the other hand, for the amorphous thin film, a positive $\gamma_s = 0.11\ \%/°C$ was found, while on the data sheet, the nominal thermal coefficient was negative $\gamma_n = -0.19\ \%/°C$. This difference between the thermal coefficients could be explained in terms of temperature effects acting on different time scales. The seasonal thermal response described by the coefficient γ_s results from the overlapping of two different competitive phenomena:

1. Small negative intrinsic thermal response (*ITR*) of the module that could be easily measured with instantaneous indoor or outdoor measurements.
2. Dominant positive temperature seasonal effect (*TSE*) that could not be measured in a laboratory because it acts on a seasonal time scale. This depends on the history of module temperature and received irradiance.

Figure 1a shows the average hourly behavior of the measured and calculated losses for different clear sky days of the four seasons obtained by the average method. Figure 1b shows the average hourly behavior of the measured and calculated thermal performance (PR_t). From Figure 1a, it can be observed that the average method reproduces quite well the overall losses on the daily and hourly time scale. On the other hand, from Figure 1b, different hourly trends between calculated and measured thermal performance are evident.

The seasonal thermal performance is well described by the measured $PR_t = (1 + \gamma_s \Delta T_{cell}(\max))$ (where $\Delta T_{cell}(\max) = \max\{\Delta T_{cell}(day)\}$), while the hourly trend is driven by the module intrinsic thermal response associated to $PR_{tn} = (1 + \gamma_n \Delta T_{cell})$. Indeed, the SWE introduces a daily bias on the negative intrinsic thermal response, and it could be estimated by the following equation:

$$\begin{aligned} PR_{ts} &= \frac{(1 + \gamma_s \Delta T_{cell}(\max))}{(1 + \gamma_n \Delta T_{cell}(\max))} \simeq (1 + \gamma_{ts} \Delta T_{cell}(\max)) \\ \gamma_{ts} &= (\gamma_s - \gamma_n) \end{aligned} \tag{14}$$

Thus, the module thermal response could be modeled by two performance factors, one varying on an instantaneous time scale and one varying on a daily time scale, reflecting the intrinsic thermal response and the seasonal SWE influence on the temperature response:

$$\begin{aligned} PR_t &= PR_{ts}(day)\, PR_{tn}(t) \\ &= (1 + \gamma_{ts} \Delta T_{cell}(\max))(1 + \gamma_n \Delta T_{cell}) \end{aligned} \tag{15}$$

Figure 1c reports a simple simulation of PR_t and PR_{tn} calculated using Equation 15 and two different temperature profiles of a winter and a summer day. For amorphous module, on a seasonal time scale, the negative *ITR* $\left(\gamma_n = -0.19\%/°C\right)$ is widely compensated by the TA effect that in Rome climatic conditions is almost two times greater ($\gamma_{ts} = (\gamma_s - \gamma_n) = 0.3\%/°C$). This leads to a positive seasonal temperature coefficient $\left(\gamma_s = 0.11\%/°C\right)$: red line in Figure 1c. On the other hand, for the technology not affected by the SWE, as the crystalline silicon, the temperature coefficients measured on an instantaneous time scale (γ_n) and on a daily time scale (γ_s) are the same: black line in Figure 1c. Thus, for any module technology, the measurement of γ_s is a method to know if there are other effects in addition to the intrinsic thermal response that affects the temperature behavior on different time scales.

Figure 1d shows the average hourly behavior of the measured and calculated thermal performance (PR_t) for different typical days of each season obtained by the separate method. On hourly and daily time scale, a good agreement between thermal performance trend on the central hours of the day (where the temperature effect is dominant) can be pointed out. On the contrary, the greater differences in the morning and the afternoon result from the spectral and reflection performance corrections or measurements. Indeed, during winter clear sky days, higher AM are reached, and in the morning and afternoon, the spectral effect becomes the dominant one. On the other hand, during summer clear sky days at an optimized monthly tilted angle, greater AOI are reached in the morning and in the afternoon, so that the reflection effect becomes dominant. Thus, not perfect modeling and difficulties in measurements could bring to great differences between the measured and calculated PR_t.

Table I reports the nominal thermal coefficients, the average seasonal coefficients and the TSE coefficients, related to Isc and Im currents (α, α'), Voc and Vm voltage (β, β') and to Pm power (γ). Because the Fill Factor (FF) temperature coefficient can be calculate as $(\alpha' + \beta') - (\alpha + \beta)$; from Table I, it appears that the module FF should not change with temperature, while on a seasonal time scale, a not negligible temperature dependence is found: $(\alpha'_s + \beta'_s) - (\alpha_s + \beta_s) = 0.095\ \left[\%/°C\right]$. This confirms that

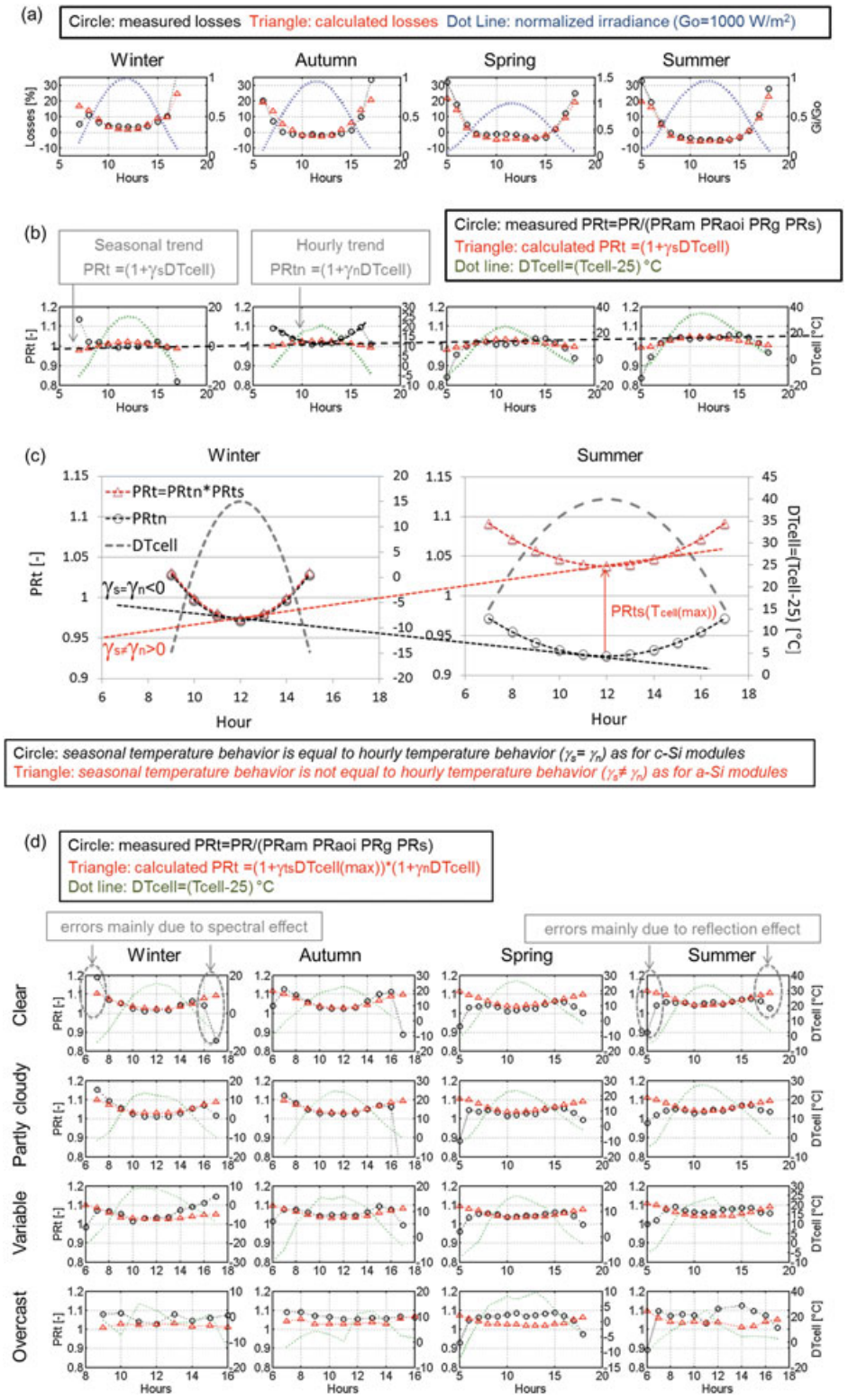

Figure 1. (a) Average hourly behavior of losses for different typical clear sky days obtained by the average method, (b) average hourly behavior thermal performance for different typical clear sky days obtained by the average method, (c) simulation of $PR_t = PR_{tn}(t)(1 + \gamma_{ts}\Delta T_{cell}(\max))$ and $PR_{tn} = (1 + \gamma_n \Delta T_{\text{cell}})$ calculated using two different temperature profiles for a winter and a summer day, (d) average hourly behavior of thermal performance (PR_t) for different typical days obtained by the separate method.

the SWE mainly affects the module FF that grows with the growing seasonal temperature. This positive FF reaction to temperature is essentially due to the greater (I_{m0}/I_{sc0}) seasonal variations.

Figure 2 shows the seasonal trend of the PR_{ts} due to the temperature seasonal effect and the trend of the PR_{tn} due to the intrinsic thermal response. The first gives an average positive contribution to the module performance with a fluctuation of 7%. The second provides an average negative impact on the PR with a fluctuation around 3%. Thus, it can be observed how the SWE compensates the intrinsic thermal response of the module producing an overall positive reaction to temperature.

3.1.2. Power seasonal effect.

The power seasonal effect takes into account only for the SWE cumulative contribution resulting from the TA and LS effects. Thus, it measures the net power gain or loss once the small negative intrinsic thermal response has been compensated by the annealing process. It is measured fitting the daily relative nominal power as follow:

$$PR_s\,(day) = \frac{P_{m0}\,(day)}{\langle P_{m0}\rangle} \simeq \frac{P^c_{m0}\,(day)}{\langle P^c_{m0}\rangle}$$
$$P^c_{m0}\,(day) = \left\langle \frac{P_m\,(G_i, T_{cell}, AM, \theta)}{(G_i/G_0)\,(PR_{am}PR_{aoi}PR_tPR_g)} \right\rangle_{day} \quad (16)$$

Table I. Nominal (from datasheet) and seasonal and temperature seasonal effect (TSE) thermal coefficients.

$\alpha_n\ [\%/^\circ C]$	$\alpha_s\ [\%/^\circ C]$	$\alpha_{ts} = (\alpha_s - \alpha_n)\ [\%/^\circ C]$
0.09	0.39	0.3
$\beta_n\ [\%/^\circ C]$	$\beta_s\ [\%/^\circ C]$	$\beta_{ts} = (\beta_s - \beta_n)\ [\%/^\circ C]$
-0.32	-0.315	-0.05
$\alpha'_n\ [\%/^\circ C]$	$\alpha'_s\ [\%/^\circ C]$	$\alpha'_{ts} = (\alpha'_s - \alpha'_n)\ [\%/^\circ C]$
0.1	0.43	0.33
$\beta'_n\ [\%/^\circ C]$	$\beta'_s\ [\%/^\circ C]$	$\beta'_{ts} = (\beta'_s - \beta'_n)\ [\%/^\circ C]$
-0.33	-0.26	-0.07
$\gamma_n\ [\%/^\circ C]$	$\gamma_s\ [\%/^\circ C]$	$\gamma_{ts} = (\gamma_s - \gamma_n)\ [\%/^\circ C]$
-0.19	*0.11*	0.3

where $P_m\,(G_i, T_{cell}, AM, \theta)$ is the power measured at $G_i \in \left\{950\frac{W}{m^2}; 1050\frac{W}{m^2}\right\}$, $\theta \in \{0^\circ; 35^\circ\}$, $AM \in \{1.2; 1.8\}$; PR_{am}, PR_{aoi} and PR_g are the spectral, reflection and irradiance corrections measured as reported in Section 2, and PR_t is the temperature correction defined in Equation 15. $\langle P^c_{m0}\rangle$ is the average value of $P^c_{m0}\,(day)$ over all the monitored period.

Figures 3 shows the PR_s and T_{cell} seasonal trends. During the initial degradation phase, the LS is the dominant effect, and around the maximum cell temperature, TA can only compensate the negative module thermal response and it lags this power degradation process. In this phase, no real shifting between the maximum of PR_s and the maximum of cell temperature can be observed, because the module was in its first days of working, and so no cumulative effect due to the absorbed energy can appear. As it will be discussed later, the PR_s in the first 2 months is overestimated, and there is not a relative maximum, but only continuous initial degradation occurs. Once the module reached its stabilized power and the daily average cell temperature grows above the $30^\circ C$, TA produces a net power regeneration, becoming the dominant effect. This process goes on increasing the module power until the cell temperature remains above $30^\circ C$. The PR_s maximum is reached in October, while the maximum temperature can be observed around the middle of August. Thus, the power seasonal effect is not in phase with temperature.

It should be remarked that from July to October, the annealing process contributes also to modify the seasonal thermal response of the module, reaching its maximum impact around the middle of August (Figure 2).

The defect density of a-Si:H increases with light exposure. TA seems to be active at low temperature under high defect density conditions or at high temperature. TA seems to be inactive at low temperature under low defect density conditions.

Nevertheless, from this separate method, it appears that the annealing process is always active, because it modifies the module thermal response on a daily time scale, increasing the performance from a minimum of 3% in winter to

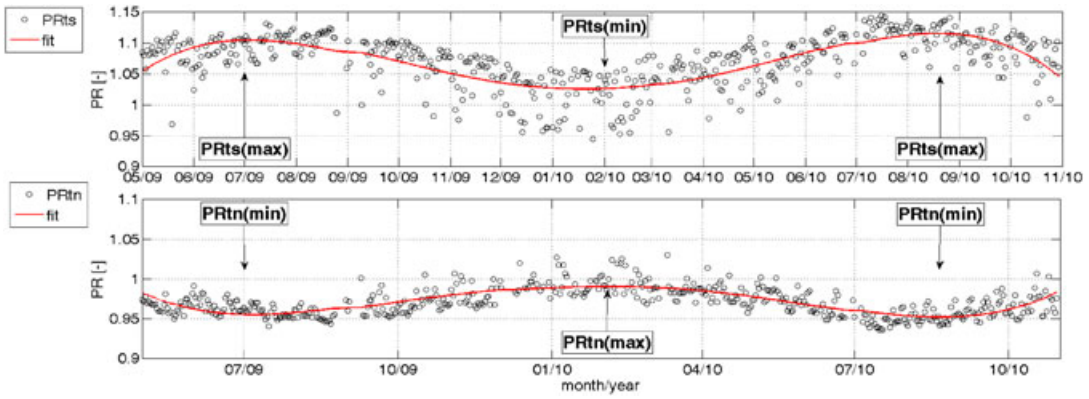

Figure 2. PR_{ts} (Temperature seasonal effect performance factor) and PR_{ts} (intrinsic thermal response performance factor) seasonal trends. PR, performance ratio.

DOI: 10.1002/pip

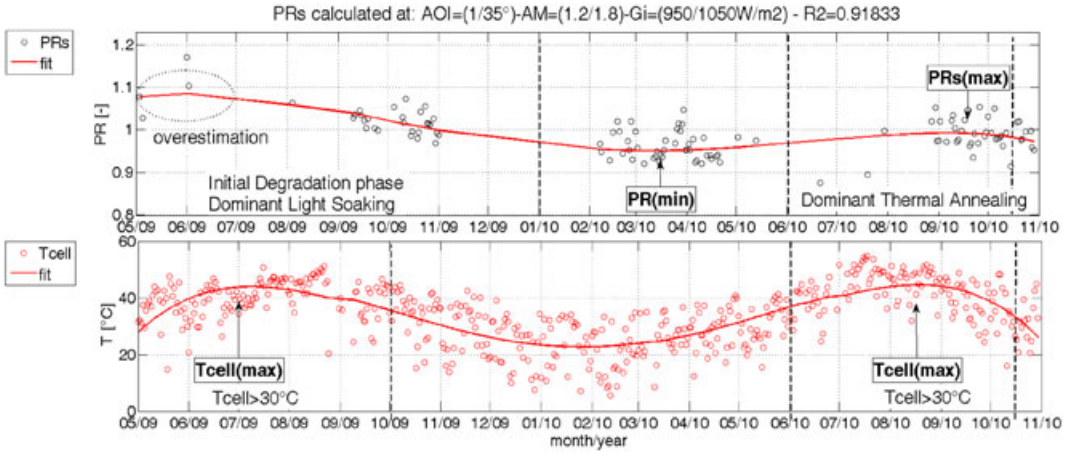

Figure 3. Power seasonal effect performance factor (PR_s) and daily average T_{cell} seasonal trends.

a maximum of 10% in summer (Figure 2). It just appears as the dominant effect when the cell temperature grows up to a fixed value that depends on the LS intensity. Near the power stabilization or at low irradiance conditions when the LS is very weak, this activation temperature could be also very low. In [5], a small power regeneration was measured at $25°C$ degree in dark condition, indicating the presence of a slow TA effect also at this temperature. Thus, the main consideration that could be confirmed from this method is that both phenomena are always present and act in a cumulative and competitive way.

This observation is coherent with the results reported in [7], finding a linear dependence of the LS power degeneration velocity from the irradiance and an exponential dependence of TA regeneration time rate from the cell temperature. Thus, the daily intensity of TA effect depends on the cell temperature frequency. So, the activation temperature could just result from the exponential temperature dependence of the TA velocity, because the intensity of this effect starts to grow dramatically when the temperature exceeds a threshold value. Moreover, this threshold value depends on the strength of LS effect and on the defects density.

3.2. Direct Method

The SW contribution to the overall seasonal performance could be evaluated trying to measure directly the relative nominal power daily variation. The nominal power could be deduced from outdoor data, fixing the variable G_i, θ and AM in a narrow range in which the relative effect can be negligible and correcting the measured power only with the ratio (G_i/G_0) and $(1+\gamma_n \Delta T_{cell})$, where γ_n is the nominal power thermal coefficient:

$$PR_{SW}(day) = \frac{P_{m0}(day)}{\langle P_{m0} \rangle} \simeq \frac{P^c_{m0}(day)}{\langle P^c_{m0} \rangle}$$
$$P^c_{m0}(day) = \left\langle \frac{P_m(G_i, T_{cell}, AM, \theta)}{(G_i/G_0)(1+\gamma_n \Delta T_{cell})} \right\rangle_{day} \quad (17)$$

where $P_m(G_i, T_{cell}, AM, \theta)$ is the power measured at $G_i \in \left\{950\frac{W}{m^2}; 1050\frac{W}{m^2}\right\}$, $\theta \in \{0°; 35°\}$, $AM \in \{1.2; 1.8\}$, and $\langle P^c_m \rangle$ is the average value of $P^c_m(day)$ over the monitored period.

Figure 4a shows the measured PR_{SW} and the relative Fill Factor seasonal trend.

As it was found with the previous method, it appears that during the initial degradation phase, LS is the dominant effect, and TA can only lag this process during the hottest seasonal period. Also in this case, the PR_{SW} in the first 2 months seems to be overestimated and there is not a relative maximum, but only continuous initial degradation occurs. The TA becomes dominant after the stabilization phase when the daily average cell temperature grows up to $30°C$. The minimum decay is reached at the beginning of March, while the maximum recovered power can be observed at the end of September. A similar result was observed in Ispra [7], with a minimum in March and a maximum in October, while in Lugano [4], minimum and maximum appears in February and in the middle of August. In Albuquerque, in NM, USA, for two a-Si tandem modules, a minimum in March and a maximum in August was found [2]. In Rome, climatic conditions and open rack installation, not considering the initial degradation, the seasonal fluctuation of the nominal power due to SWE is around 8%. Moreover, Figure 4a shows that the SWE is driven essentially by the fill factor changes, because I_m and V_m show greater seasonal variations with respect to I_{sc} and V_{oc}. The same result was found in [7], by laboratory-controlled conditioning of an a-Si module and in [16] in outdoor conditions.

To verify the reliability of the PR_{SW}, it is important to prove that it could not be sensibly affected by other effects. Because the POA irradiance is fixed in a narrow range near G_0: $G_i \in \left\{950\frac{W}{m^2}; 1050\frac{W}{m^2}\right\}$ and the power is corrected by (G_i/G_0), the PR_{SW} measurements could not be affected by the irradiance effect. Also, the reflection should not affect these measurements because AOI is fixed in a range $\theta \in \{0°; 35°\}$, where the reflection

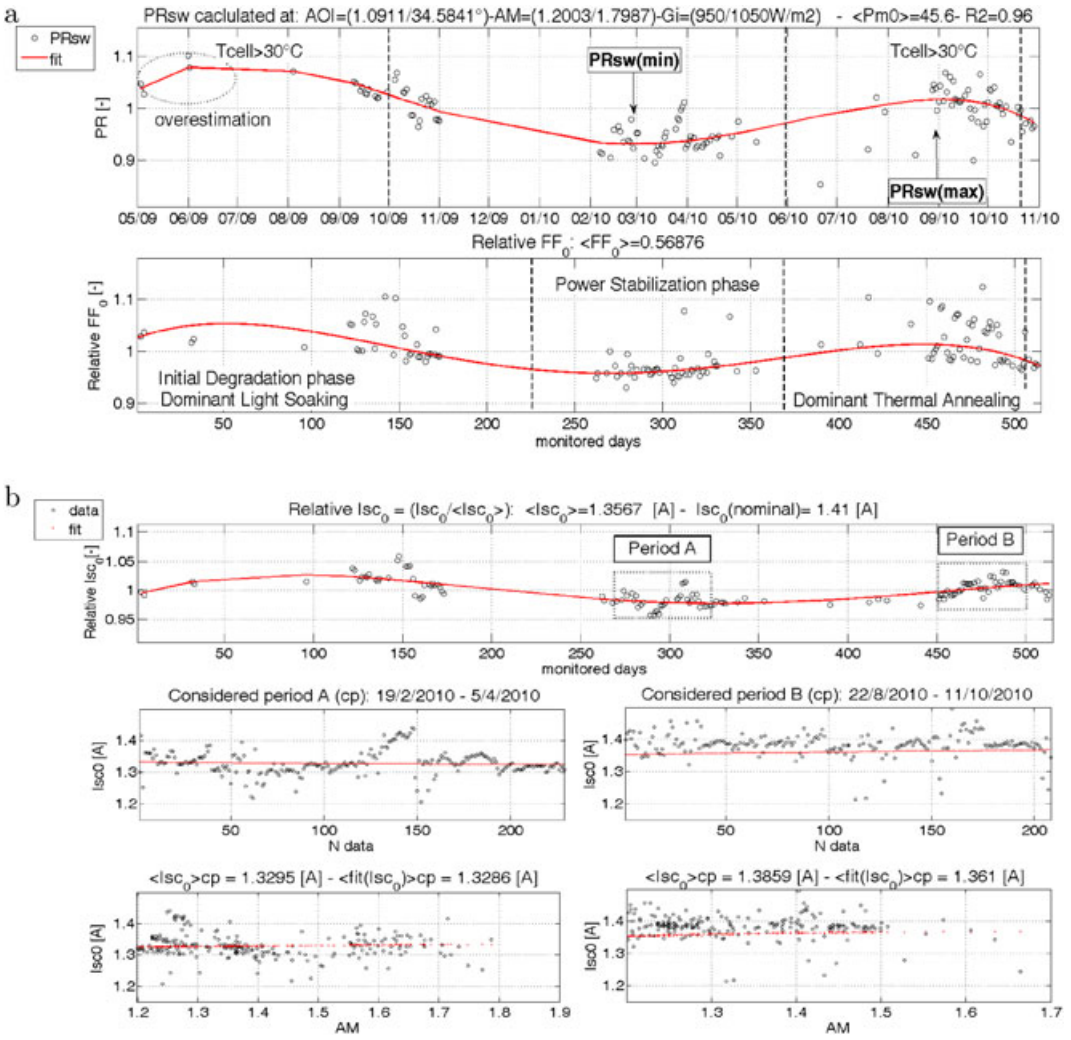

Figure 4. (a) Measured PR_{SW} (Staebler–Wronsky Effect performance factor) and the relative fill factor seasonal trend, (b) seasonal fluctuations of the relative daily I_{sc0} current and instantaneous behavior of I_{sc0} measured in two different periods.

effect is negligible. Furthermore, the temperature effect has been corrected using the nominal thermal coefficients. Thus, only the spectral effect could influence the SW performance. For all the a-Si modules, the spectral mismatch, due to a large air mass, strongly affects the performance (high energy gap), and this is even stronger in multi-junctions devices. Moreover, for multi-junction cells, the mismatch between the junction photogenerated currents causes a performance loss also at AM near to one, corresponding to bluer spectrum (this is known as secondary spectral effect). Figure 4b shows the seasonal fluctuations of the relative daily I_{sc0} current: $PR_{SW}^{Isc} = I_{sc0}(day) / \langle I_{sc0} \rangle$, where $I_{sc0}(day) = \left\langle \frac{I_{sc}(G_i, T_{cell}, AM, \theta)}{(G_i/G_0)(1+\alpha_n \Delta T_{cell})} \right\rangle_{day}$ measured at $G_i \in \left\{950\frac{W}{m^2}; 1050\frac{W}{m^2}\right\}$, $\theta \in \{0°; 35°\}$, $AM \in \{1.2; 1.8\}$ and $\langle I_{sc0} \rangle$ is the average $I_{sc0}(day)$ over all the monitoring period. Then, also the instantaneous behavior of $I_{sc0} = \frac{I_{sc}(G_i, T_{cell}, AM, \theta)}{(G_i/G_0)(1+\alpha_n \Delta T_{cell})}$ measured in two periods is reported and plotted versus the numbers of data (in a time sequence) and versus AM. In both the selected periods the PR_{SW} is almost constant: period A is during the stabilization phase, while period B is during the maximum TA recovery phase. No direct dependence of I_{sc0} from AM can be observed, because it appears fluctuating around a constant value $\langle I_{sc0} \rangle_{cp}$. Thus, in the range $AM \in \{1.2; 1.8\}$, the spectral effect could be considered negligible. In period A, the fitting curve PR_{SW}^{Isc} well approximates the average I_{sc0} measurements $\left(\langle I_{sc0} \rangle_{cp}\right)$, while in period B, it gives a small underestimation. The great fluctuations of I_{sc0} at fixed AM mainly depend on irradiance instability. If only the I-V curve at stable irradiance (not varying more then 1% during 2 min before and after the measurement) are selected, much smaller fluctuations are found.

3.3. Comparison between methods

Figure 5 reports the comparison between the measured and calculated daily performance for the two methods

DOI: 10.1002/pip

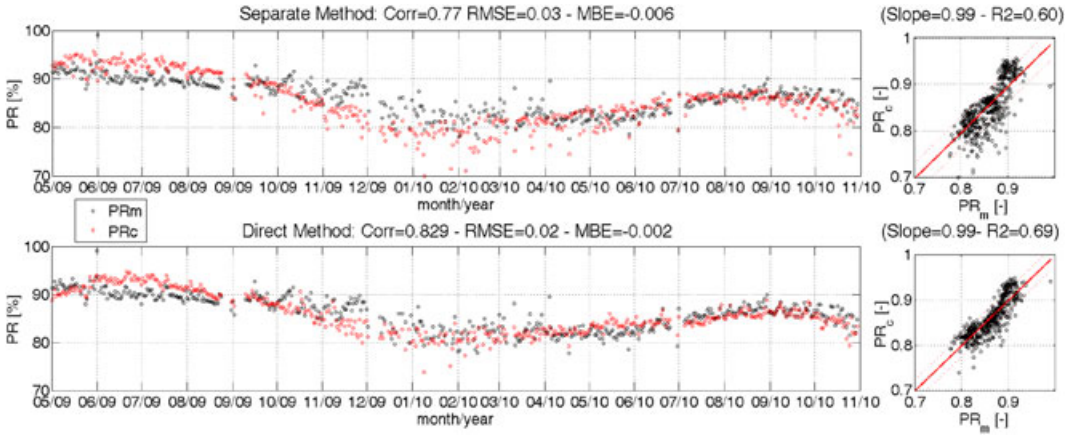

Figure 5. Comparison between the measured (PR_m) and calculated (PR_c) daily performance.

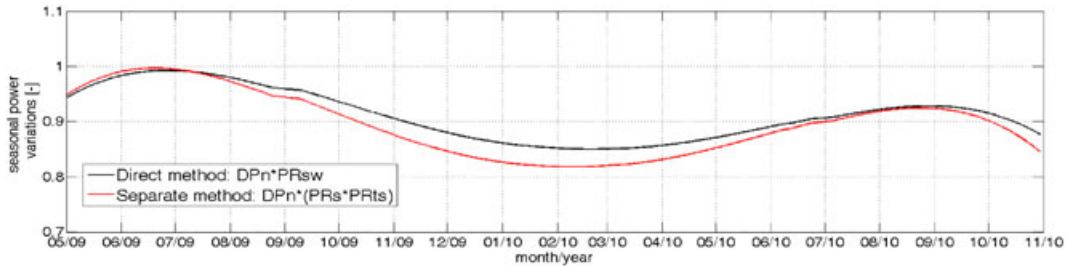

Figure 6. Staebler–Wronsky evaluation obtained by the two methods.

(Equation 11). Both methods give comparable results, showing to be able to reproduce the measured performance. The most evident errors are in the initial degradation phase, where first an overestimation and then a small underestimation are observed. Also, a small overestimation in the first annealing period can be pointed out. It can be seen from Figures 3 and 4a that these errors greatly depend on the lack of data for the PR_s and PR_{SW} interpolations. However, the direct method shows a greater correlation coefficient and a smaller RMSE ($Corr = 83\% - RMSE = 0.02$) with respect to the separate method ($Corr = 77\% - RMSE = 0.03$).

Figure 6 compares the SW evaluation obtained by the two methods. Both the approaches give a similar trend behavior. A good agreement is found in summer time, but in the whole, the separate method gives an underestimation of the SW performance that reaches a maximum of 3% in winter time. This could depend on the overestimation of the annealing impact on the temperature behavior in the cold, variable and overcast days (Figure 1d).

It should be remarked that the estimated coefficients of the parametric functions, described in subsection 2.2, depend on the method used to evaluate the SWE. Indeed, the temperature correction PR_t used to translate the experimental measurements to STC temperature should include not only the intrinsic thermal response of the DUT (and so the nominal thermal coefficients $\alpha_n, \beta_n, \gamma_n$ etc.) but also the SWE contribution. Thus, for instance, the *Isc* thermal correction used in Equations 6,7, and 9 is calculated as:

- $PR_t^{Isc} = (1 + \alpha_n \Delta T_{cell})\,(1 + \alpha_{ts} \Delta T_{cell}\,(\max))$ (defined in equation 15) for the separate method
- $PR_t^{Isc} = (1 + \alpha_n \Delta T_{cell})\, PR_{SW}^{Isc}$ for the direct method, where PR_{SW}^{Isc} is the seasonal variation of the relative short circuit current $\frac{I_{sc0}(day)}{\langle I_{sc0} \rangle}$ measured with the same method used for PR_{SW} evaluation and reported in Figure 4b.

These coefficients are reported in the appendix. It can be noticed that with the two methods, very similar coefficients were estimated. Moreover, the coefficients CB (AMM interpolation) and CC (IAM interpolation) can be compared with the ones measured by Sandia Laboratory using a different technique (CBk and CCk, reported in the appendix). Also in this case, a good agreement could be found.

Finally, it should be pointed out that the irradiance performance model described in Equation 10 reproduces with high accuracy the irradiance response of c-Si module, as reported in [12], improving the correlation between measured and calculated daily PR of 10%. On the other hand, for a-Si thin film module, it does not well describe the behavior at low irradiance levels, and at high irradiance, it shows to be too sensible to the C_3 coefficient value.

For this amorphous module, no power loss for series resistance $\left(R_{\text{series}} I_m^2\right)$ seems visible so the slope of PR_g at high irradiance is very flat. Thus, a small variation of 1% of C_3 coefficient that, as expected, is very close to one produces a variation of 1% of the annual irradiance losses or gains: C_3 = 1.01 produce around 1% of gain (as in [12]), while C_3 = 0.99 produce 1% of loss (as in the DM method). Thus, the estimated irradiance losses or gains for this thin film cannot be considered reliable. Nevertheless, these losses or gains are almost constant and very small (around 1%). Probably, for this reason, the irradiance effect was not considered in the PR analysis reported in [4].

4. SEASONAL PERFORMANCE BEHAVIOR ANALYSIS

In this section, the PR and losses analysis are discussed using the SWE performance factor measured with the direct method. For this analysis, the technique described in subsection 2.4 is used to calculate the impact of the different effects (loss fraction LF_i) both on the all monitoring period performance and on the daily time scale.

Table II reports the performance ratio and losses measured and calculated with the direct method over the monitoring periods: from 1 May 2009 to 10 October 2010 and

Table II. Performance ratio and losses over the monitored period.

	EPV50
PR_m	86.6%
L_m	13.4%
PR_c	86.7%
L_c	13.3%
$LF_{\Delta Pn}$	*8,7%*
LF_{SW}	*-1.5 %*
LF_t	*3.5%*
LF_{am}	*0.2 %*
LF_{aoi}	*1.2%*
LF_g	*1.2%*

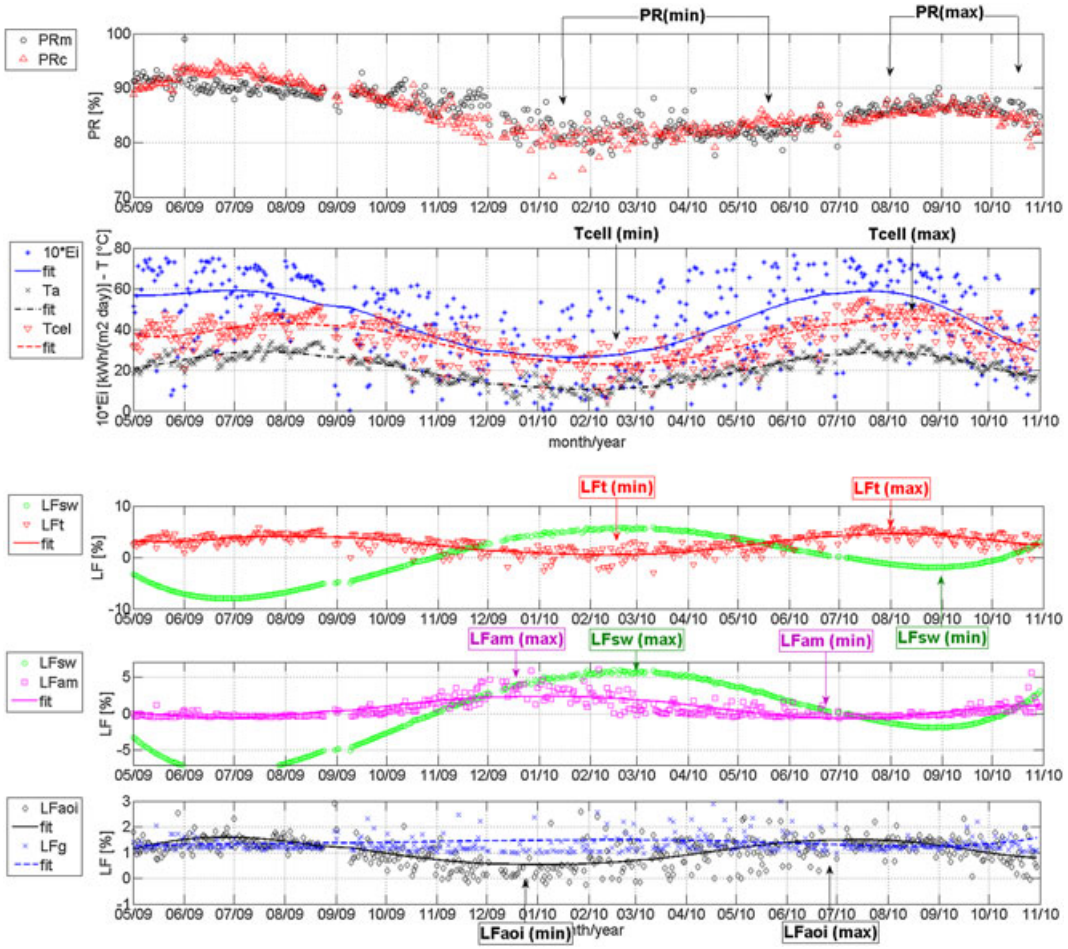

Figure 7. Performance ratio (PR) and loss fraction daily behavior obtained with the direct method.

DOI: 10.1002/pip

a very good agreement can be pointed out. Then, also the losses fractions, defined in Equation 12, were calculated.

The main loss is the average degradation of the nominal power $\left(LF_{\Delta Pn} = 8,7\%\right)$ followed by temperature loss due to the small negative intrinsic thermal junction response ($LF_t = 3.5\%$). On the whole period, the SWE brings a small gain of ($LF_{SW} = -1.5\%$), while the other effects do not have a big impact on the loss calculated on all the monitored period. It should be remarked that the reflection effect has a very small impact, because the tilt angle was changed every month of the monitoring period to optimize the energy production. This allows to measure the incident angle relative response from outdoor data but obviously minimizes the reflection effect. Moreover, as discussed in subsection 3.3, the irradiance loss fraction cannot be considered a reliable estimation.

Figure 7 shows the PR and loss fractions daily behavior. It can be observed that in spite of the small annual impact, the SW and the spectral effect play an important role on the daily time scale. According to [4], spectral effect has a maximum in winter solstice with longer air mass and redder spectrum and a minimum in summer solstice with bluer spectrum, with a fluctuation around 4%. In the climatic conditions of Rome, SW effect has a maximum in the late winter when the higher LS degradation is reached, and a minimum in the late summer when the TA effect reaches the higher power recovery. Excluding the initial degradation phase, the annual fluctuation (LF_{SW} (max) – LF_{SW} (min)) is around 7%. In [16] was found that SW effect can produce seasonal fluctuation of the peformance of silicon thin films up to 4-6%. Temperature effect due to the intrinsic thermal junction response has a maximum in middle August at the higher daily temperature and a minimum between February and March, at lower daily temperature, with a 4% of fluctuations. Reflection effect realizes its maximum and minimum impact during summer and winter solstice when the highest and lowest daily maximum incident angle is reached. Indeed, in this case, the AOI was kept to its optimum monthly value, and so, the reflection loss takes into account only the loss due to the AOI hourly variations. Thus, because of the optimal tilt in summer, greater angles of incidence are reached, and so, a greater reflection loss is realized. In the reporting installation feature, the annual fluctuation is very small, around 1%. Thus, the wide PR minimum range results from the overlapping of the spectral and SW losses that are much higher then the reflection and temperature effect. On the other hand, the PR maximum range depends essentially on the SW effect in its maximum TA recovery phase, which reduces the negative temperature and reflection impact. Thus, it was confirmed in a quantitative way that the increase of the a-Si module performance in summer and the decrease in winter depend on the LS, TA and spectral effects that are able to compensate the negative intrinsic thermal response of the module. In Rome climatic conditions, low latitude and prevalent warm weather, the SW is the dominant effect. On the contrary, in other sites with higher latitude or prevalent cold weather, the spectral effect could be the dominant one.

On the whole, in the reported real operating conditions for the amorphous technology, the competitive impacts of spectral, SW, temperature and reflection effects produce

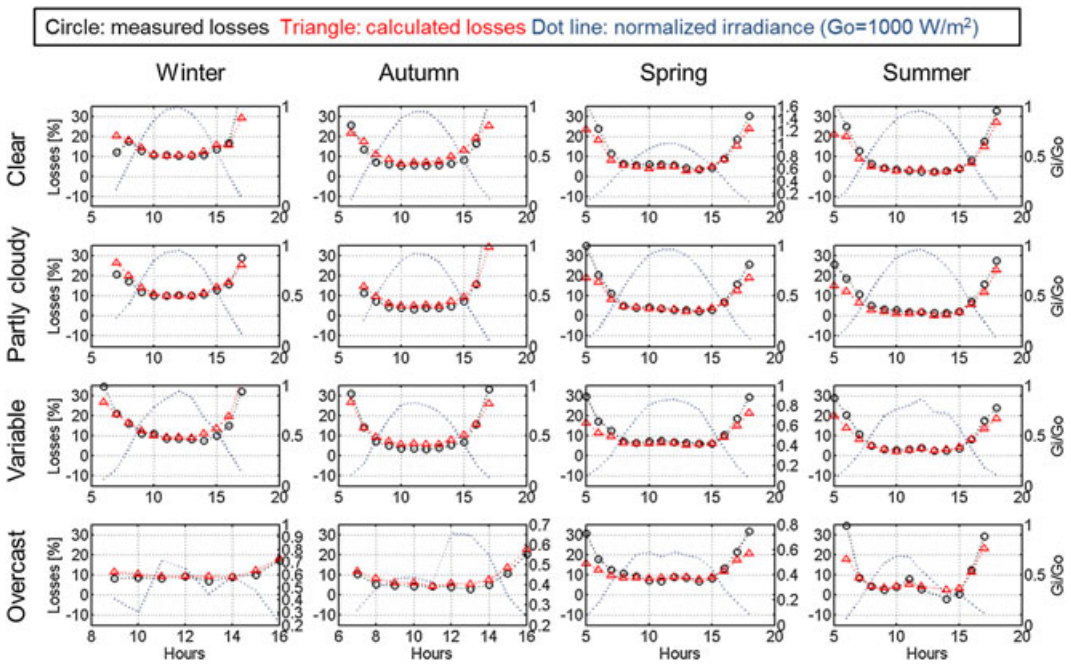

Figure 8. Measured (black) and calculated (red) hourly losses: $L = (1 - PR)$ for different typical days obtained with the direct method.

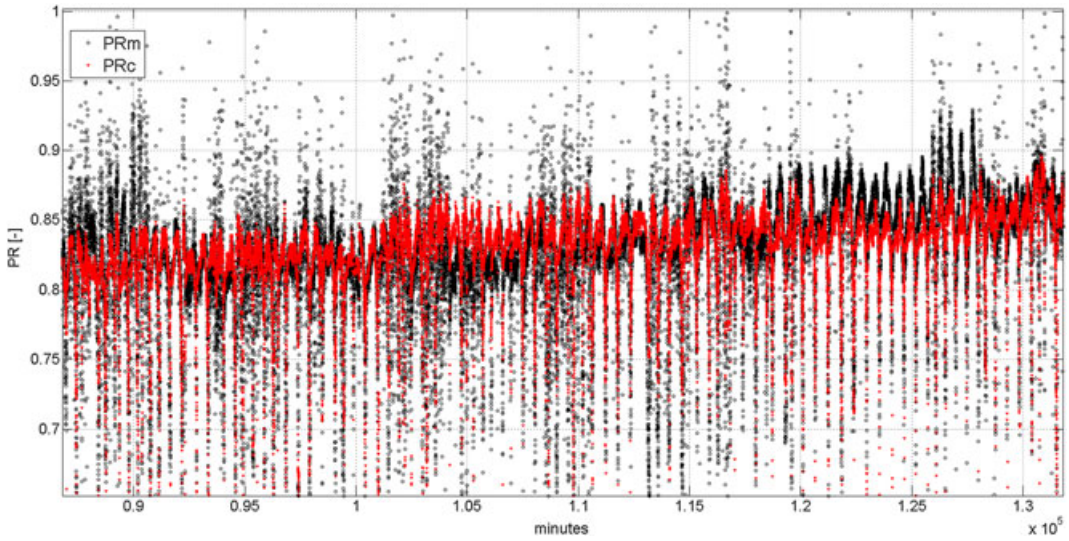

Figure 9. Sample of the instantaneous measured (PR_m) and calculated (PR_c) performance ratio (PR) obtained with the direct method.

small yearly PR fluctuations less then 10% (excluding the initial degradation phase).

Figure 8 reports the direct method measured and calculated hourly losses for different typical days obtained, averaging the minutes value of each cluster of days and then calculating the hourly values. It can be observed that the model reproduces quite well the average hourly measured losses for all the cluster of days. Again, it can be pointed out that the greater differences between measured and calculated losses in the early morning and late afternoon results from the spectral and reflection imperfect modeling and difficulty in measurements.

Figure 9 shows a sample of the instantaneous measured and calculated performance ratio. The model reproduces the PR trend with an acceptable level of accuracy also on the minute time scale. The greater error essentially depends on the nominal power daily variation that has been statistically evaluated using a too small day sample. Moreover, the great variability of the measured PR around midday mainly depends on the irradiance instability not correctly followed by the MPP tracking. Indeed, the model that is not affected by this effect does not show this phenomenon.

5. CONCLUSIONS

Two different methods to measure the SW impact on the seasonal performance ratio of a double junction amorphous silicon module are presented. The first method provides a separate evaluation of the TA contribution to the seasonal thermal response and of the SW cumulative impact on the seasonal performance. The second method provides a direct measurement of the SW effect. Both methods bring similar results, even if the second leads to a slightly better modeling of measured performance and losses.

With the first method, it is possible to show, in a quantitative way, how the TA modifies the seasonal thermal response of the module so that it appears to react positively to the seasonal temperature even if its power thermal coefficient is negative. Thus, the results in [1] are explained using a different approach. Moreover, an increase of the performance from a minimum of 3% in winter to a maximum of 10% in summer due to the TA direct impact on the temperature behavior is measured. Thus, this effect seems always active, confirming the results obtained by M. Nikolaeva-Dimitrova *et al.* in [7]. The activation temperature of the TA process could just be a consequence of the exponential temperature dependence of the TA velocity of power recovery, LS strength and defects density. In outdoor measurements, this threshold temperature appears when the TA process becomes dominant with respect to the LS effect at a high level of defects concentration that is around a daily average cell temperature of $30^{\circ}C$ for the reported case.

With the second method, the direct impact of the SW effect on the seasonal performance is evaluated. Even if only the initial degradation and the temperature effect produces relevant losses on the whole monitoring period (8,7% and 3.5%), spectral and SWE can produce great daily losses or gains. In the reporting site and installation features, the performance time behavior (on a daily basis) cannot be understood without these effects. Spectral effect has a minimum in winter solstice and a maximum in summer solstice with a fluctuation around 4%, while SWE has a maximum in the late winter and a minimum in the late summer with an annual fluctuation around 7%. It has been found that the minimum performance results from the overlapping of spectral and SWE (during the dominant LS degradation phase), while the maximum performance is produced by the action of SWE (during the dominant TA regeneration phase) that reduces the temperature losses. Thus, it has been confirmed that for the a-Si modules, the higher performance in summer and the lower

performance in winter depend both on SW and spectral effects. In Rome climatic conditions, the SW is the dominant effect, while in other real operating conditions, the spectral effect could be the dominant one. On the whole, in the amorphous technology, the competitive impacts of SW, spectral and temperature effects produce small seasonal PR fluctuations (less than 10% excluding the degradation phase).

Finally, it should be remarked that the PR model reported in this work cannot be used for a-Si modules performance estimation but only for the performance analysis, because a SWE semi-empirical model is not available at this stage. The separate model could be a first step in this direction.

6. NOMENCLATURE

Abbreviations

STC	Standard test condition
POA	Plane of the array
AOI	Angle of incidence
AM	Air mass
ROC	Real operating condition
DUT	Device under test
LS	Light soaking
TA	Thermal annealing
SWE	Staebler–Wronsky effect
SM	Separate method
DM	Direct method
TSE	Temperature seasonal effect
ITR	Intrinsic thermal response
PSE	Power seasonal effect

Variables

$\{G_0, AM_0, \theta_0, T_0\} = \left\{1000\frac{W}{m^2}, 1.5G, 0°, 25°C\right\}$	STC values for POA irradiance, air mass, angle of incidence, cell temperature
G_i	Plane Of Array irradiance $\left[\frac{W}{m^2}\right]$
G^{dni} and $G_i^d = G^{dni}\cos(\theta)$	Direct normal amd POA irradiance $\left[\frac{W}{m^2}\right]$
$G_i^{sh} = G_i - G_i^d$	Diffuse POA irradiance $\left[\frac{W}{m^2}\right]$
$CR_i = G_i^{sh}/G_i$	POA cloud ratio [–]
$AM = \frac{e^{(-.0001184)h}}{\cos(Zs)+0.5057(96.08-Zs)^{-1.634}}$	air mass [–] with Zs = zenith angle $\left[°\right]$ and h =site altitude $\simeq$ 100 m
θ	incidence angle $\left[°\right]$;
T_{bom}	back of module temperature $\left[°C\right]$
ΔT_0	difference between T_{bom} and the reference cell temperature at $1000\frac{W}{m^2}\left[°C\right]$
$\Delta T_{cell} = T_{bom} + \Delta T_0\left(\frac{G_i}{G_0}\right)$ –25	difference between cell temperature and $25°C$ $\left[°C\right]$
$\{I_{sc0}, V_{oc0}, P_{m0}, I_{m0}, V_{m0}\}$	short circuit current, open circuit voltage and maximum power, current and voltage measured at STC
$PR = \eta_{ROC}/\eta_{STC} = \frac{P_m}{Pn}/\frac{G_i}{G_0}$	Perfomance Ratio [–]

ACKNOWLEDGEMENTS

Dr. Marco Pierro and Dr. Francesco Bucci are supported in the frame of the research Project no. 21 (DSP Project) financed by an agreement between the Italian Ministry of the Economic Development (MISE), the Italian Trade Promotion Agency (ICE) and the Conference of the Deans of the Italian Universities (CRUI). This work is also supported by the Lazio Region within the frame of the Centre for Hybrid and Organic Solar Energy (CHOSE).

REFERENCES

1. Ishii T, Otani K, Takashima T, Kawai S. Estimation of the maximum power temperature coefficients of PV modules at different time scales. *Solar Energy Materials & Solar cells* 2011; **95**: 386–389.
2. King DL, Kratochvil JA, Boyson WE. Stabilization and performance characteristics of commercial amorphous-silicon PV modules, In *Proceeding of the 28th IEEE PVSC*, Anchorage, USA, 2000; 1446–1449.
3. Gottschalg R, del Cueto J, Betts TR, Williams SR, Infield DG. Investigating the seasonal performance of amorphous silicon single and multi-junction modules, In *Proceedings of the 3rd World Conference on Photovoltaic Energy Conversion,* Vol. 2, Osaka, Japan, 2003; 2078–2081. ISBN: 4-9901816-0-3.
4. Fanni L, Virtuani A, Chianese D. A detailed analysis of gain and losses of a fully integrated flat roof amorphous silicon photovoltaic plant. *Solar Energy* 2011; **85**: 2360–2373.
5. Virtuani A, Fanni L. Seasonal power fluctuations of amorphous silicon thin-film solar modules:distinguishing between different contributions. *Progress in Photovoltaics: Research and Applications* 2014; **22**(2): 208–217.
6. Pearce JM, Deng J, Albert ML, Wronski CR, Collins RW. Room temperature annealing of fast states from 1

sun illumination in protocrystalline Si:H materials and solar cells, In *31st IEEE Photovoltaic Specialists Conf. Proc.,* IEEE, Lake Buena Vista, Florida, USA, 2005; 1536–1539.
7. Nikolaeva-Dimitrova M, Robert K, Ewan D. Controlled conditioning of a-Si:H thin film modules for efficiency prediction. *Thin Solid Films* 2008; **516**: 6902–6906.
8. Wohlgemuth JH, Ransome SJ. Performance of BP solar tandem junction amorphous silicon modules, In *Proceedings of 29th IEEE-PVSEC*, New Orleans, USA, 2002; 1142–1145.
9. Gottschalg R, Betts TR, Infield DG, Kearney MJ. The effect of spectral variations on the performance parameters of single and double junction amorphous silicon solar cells. *Solar Energy Materials & Solar Cells* 2005; **85**: 415–428.
10. Williams SR, Beyer HG, Gottschalg R, Betts TR, Infield DG. Modelling long-term module performance based on realistic reporting conditions with consideration to spectral effects, In *Proceedings of 3rd World Conference on Photovoltaic Energy Conversion,* Vol. 2, Osaka, Japan, 2003; 1908–1911. ISBN:4-9901816-0-3.
11. Cornaro C, Andreotti A. Influence of Average Photon Energy index on solar irradiance characteristics and outdoor performance of PV modules. *Progress in Photovoltaic: Research and Applications* 2013; **21**(2): 996–1003.
12. Pierro M, Bucci F, Cornaro C. Full characterization of PV modules in real operating conditions: theoretical model, measurement method and results. *Progress in Photovoltaics: Research and Applications* 2014. Published online in Wiley On-line Library DOI:10.1002/pip.2450.
13. Spena A, Cornaro C, Serafini S. Outdoor ESTER test facility for advanced technologies PV modules, In *Proceedings of the 33rd IEEE PV Specialists Conference*, San Diego (CA), May 11–16 2008; 1–5.
14. Kolodziej A. Staebler–Wronski effect in amorphous silicon and its alloys. *Opto-Electronics Review* 2004; **12**(1): 21–32.
15. King DL, Kratochvil JA, Boyson WE. Field experience with a new performance characterizations procedure for photovoltaic arrays, In *Proceedings 2nd World Conference and Exhibition on Photovoltaic Solar Energy Conversion*, Vienna, Austria, 1998; 1947–1952.
16. Ishii T, Otani K, Takashima T, Xue Y. Solar spectral influence on the performance of photovoltaic (PV) modules under fine weather and cloudy weather conditions. *Progress in Photovoltaics: Research and Applications* 2013; **21**(4): 481–489.

APPENDIX A: MEASURED PARAMETERS

Table A1. Measured parameters (CA and CB) and Sandia laboratory parameters(CBk) for the CRM and AMM functions.

CA (*SM*)	CB (*SM*)	CA (*DM*)	CB (*DM*)	CBk
1.09	9.23 E-1	1.044	9.62 E-1	9.67 E-1
-1.24 E-1	7.39 E-2	-6.87 E-2	2.26 E-2	6.31 E-2
	-1.81 E-2		7.48 E-3	-3.37 E-2
	-4.52 E-4		-5.79 E-3	3.14 E-3
	2.37 E-5		4.45 E-4	9.211 E-5

Table A2. Measured parameters (CC) and Sandia laboratory parameters(CCk) for the IAM function.

CC (*SM*)	CC (*DM*)	CCk
1	1	1
-1.47 E-3	-1.51 E-3	-2.44 E-3
2.75 E-4	2.80 E-4	3.10 E-4
-1.45 E-5	-1.46 E-5	-1.25 E-5
2.71 E-7	2.71 E-7	2.11 E-7
-1.72 E-9	-1.72 E-9	-1.36 E-9

Table A3. Measured parameters (C) for the irradiance effect modellization.

C (*SM*)	C (*DM*)
-1.51 E-2	2.69 E-4
-2.08 E-2	-1.57 E-2
9.99 E-1	9.90 E-1